

LETTER • **OPEN ACCESS**

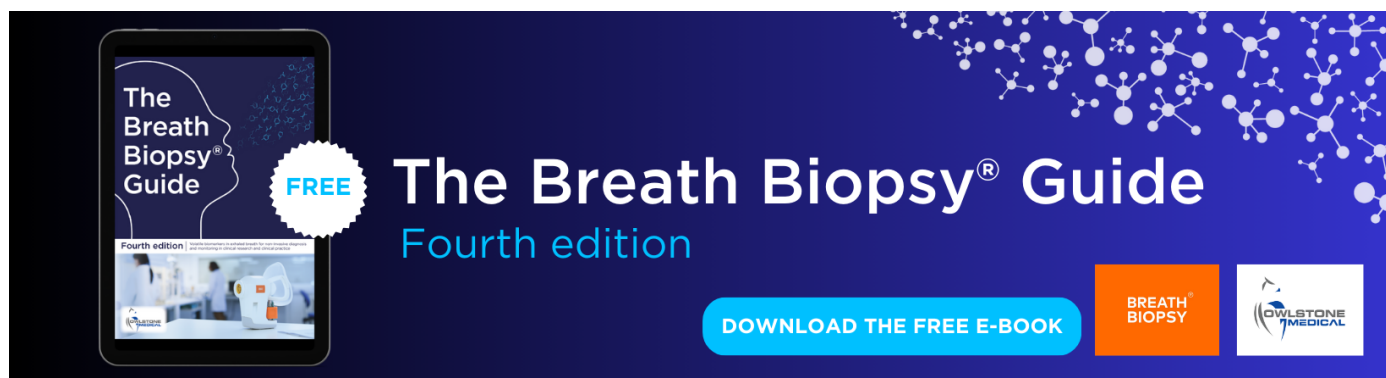
## Placing the east-west North American aridity gradient in a multi-century context

To cite this article: Daniel A Bishop *et al* 2021 *Environ. Res. Lett.* **16** 114043

View the [article online](#) for updates and enhancements.

You may also like

- [Emergent constraints on tropical atmospheric aridity—carbon feedbacks and the future of carbon sequestration](#)  
Armineh Barkhordarian, Kevin W Bowman, Noel Cressie *et al.*
- [Belowground soil and vegetation components change across the aridity threshold in grasslands](#)  
Zhuobing Ren, Changjia Li, Bojie Fu *et al.*
- [Distinct vegetation response to drying and wetting trends across an aridity threshold](#)  
Wei Zhao, Xiubo Yu, Yu Liu *et al.*



The Breath Biopsy® Guide  
Fourth edition

FREE

DOWNLOAD THE FREE E-BOOK

BREATH BIOPSY

OWLSTONE MEDICAL

ENVIRONMENTAL RESEARCH  
LETTERS

## LETTER

Placing the east-west North American aridity gradient  
in a multi-century context

## OPEN ACCESS

RECEIVED  
25 July 2021REVISED  
20 September 2021ACCEPTED FOR PUBLICATION  
13 October 2021PUBLISHED  
8 November 2021

Original content from  
this work may be used  
under the terms of the  
[Creative Commons  
Attribution 4.0 licence](#).

Any further distribution  
of this work must  
maintain attribution to  
the author(s) and the title  
of the work, journal  
citation and DOI.



Daniel A Bishop<sup>1,2,\*</sup> , A Park Williams<sup>1,3</sup> , Richard Seager<sup>4</sup> , Edward R Cook<sup>1</sup> , Dorothy M Peteet<sup>4,5</sup> , Benjamin I Cook<sup>1,5</sup> , Mukund P Rao<sup>1,6,7</sup> and David W Stahle<sup>8</sup>

<sup>1</sup> Tree Ring Laboratory, Lamont-Doherty Earth Observatory of Columbia University, Palisades, NY 10964, United States of America

<sup>2</sup> Department of Earth and Environmental Sciences, Columbia University, New York, NY 10027, United States of America

<sup>3</sup> Department of Geography, University of California, Los Angeles, CA 90095, United States of America

<sup>4</sup> Lamont-Doherty Earth Observatory of Columbia University, Palisades, NY, 10964, United States of America

<sup>5</sup> NASA Goddard Institute for Space Studies, New York, NY 10025, United States of America

<sup>6</sup> Cooperative Programs for the Advancement of Earth System Science, University Corporation for Atmospheric Research, Boulder, CO 80301, United States of America

<sup>7</sup> Department of Plant Science, University of California, Davis, CA 95616, United States of America

<sup>8</sup> University of Arkansas, Fayetteville, AR 72701, United States of America

\* Author to whom any correspondence should be addressed.

E-mail: [daniel.bishop98@gmail.com](mailto:daniel.bishop98@gmail.com)

**Keywords:** drought, soil moisture, precipitation, aridity gradient, North America, tree-ring reconstruction

Supplementary material for this article is available [online](#)

**Abstract**

Instrumental records indicate a century-long trend towards drying over western North America and wetting over eastern North America. A continuation of these trends into the future would have significant hydroclimatic and socioeconomic consequences in both the semi-arid Southwest and humid East. Using tree-ring reconstructions and hydrologic simulations of summer soil moisture, we evaluate and contextualize the modern summer aridity gradient within its natural range of variability established over the past 600 years and evaluate the effects of observed and anthropogenic precipitation, temperature, and humidity trends. The 2001–2020 positive (wet east-dry west) aridity gradient was larger than any 20 year period since 1400 CE, preceded by the most negative (wet west-dry east) aridity gradient during 1976–1995, leading to a strong multi-decade reversal in aridity gradient anomalies that was rivaled only by a similar event in the late-16th century. The 2001–2020 aridity gradient was dominated by long-term summer precipitation increases in the Midwest and Northeast, with smaller contributions from more warming in the West than the East and spring precipitation decreases in the Southwest. Multi-model mean climate simulations from Coupled Model Intercomparison Project 6 experiments suggest anthropogenic climate trends should not have strongly affected the aridity gradient thus far. However, there is high uncertainty due to inter-model disagreement on anthropogenic precipitation trends. The recent strengthening of the observed aridity gradient, its increasing dependence on precipitation variability, and disagreement in modeled anthropogenic precipitation trends reveal significant uncertainties in how water resource availability will change across North America in the coming decades.

**1. Introduction**

Global climate change is projected to exacerbate drought severity and extent (Cook *et al* 2020) and increase precipitation extremes through the 21st century (Singh *et al* 2013). In North America, extreme

precipitation and drought risk have increased in many regions and are projected to increase in response to anthropogenic climate change through the 21st century (Seager 2007b, Williams 2013, Cook *et al* 2014, 2015, Bishop *et al* 2019a). Anthropogenic warming has likely exacerbated western drought severity

and contributed to one of the most severe droughts in southwestern North America in 1200+ years (Williams *et al* 2020).

In sharp contrast, eastern North America experienced positive precipitation and reduced warming trends over the past century (Hartmann 2013, Easterling 2017, Mascioli *et al* 2017). Increased precipitation has been linked to midlatitude Rossby wave patterns in the Northeast (Seager *et al* 2012), the North Atlantic Subtropical High (NASH) in the Southeast (Li *et al* 2012), and land use change and the Great Plains low-level jet in the Midwest and Northern Plains (Barandiaran *et al* 2013, Mueller *et al* 2016). Cooling or reduced warming trends in the Southeast and Midwest have been linked to land use change (Mueller *et al* 2016, Nikiel and Eltahir 2019), natural climate variability (Partridge 2018), aerosol emissions (Lebensperger 2012, Yu 2014, Mascioli *et al* 2017), and evaporative cooling from increased precipitation and reforestation (Pan *et al* 2004, Portmann *et al* 2009, Zhang 2020). Regardless of the origin, the combined increases in precipitation and reduced warming have increased soil moisture in eastern North America.

Eastern wetting and western drying have strengthened the east-west North American soil moisture gradient during a period of enhanced global anthropogenic warming with far-reaching impacts. The yield, spatial distribution, and type of cropland and natural vegetation are particularly vulnerable to soil moisture and drought variability (Wang 2014, Seager *et al* 2018a). Precipitation and moisture transport are affected by upwind soil moisture availability, which impacts drought propagation (or reversal) in adjacent regions (Seneviratne *et al* 2010, Herrera-Estrada *et al* 2019). Soil moisture gradients also moderate regional climate through convection and tornadic activity (Lanicci *et al* 1987, Gensini and Brooks 2018) and large-scale circulation and storm tracks (Pal and Eltahir 2003, Zhou 2021). Sustained changes in the spatial gradient of soil moisture across North America therefore have the potential to alter the climatology and variability of these systems.

The aridity gradient was previously identified as a major mode of annual-to-decadal drought and circulation variability over North America since 900 CE (Woodhouse *et al* 2009). The divide of the humid east and arid west has persisted in North American climatology and is often stated to be near the 100th meridian. The divide has experienced shifts during the early-to-mid Holocene (Webb *et al* 1983, Baker *et al* 2002) and is projected to shift east by the late-21st century in response to anthropogenic increases in evaporative demand, although the strength of the aridity gradient is projected to weaken (Seager *et al* 2018a, 2018b).

Tree-ring reconstructions of drought and soil moisture across North America have been used to

evaluate and contextualize observed and projected extremes in drought and pluvial events (e.g. Touchan *et al* 2008, Cook *et al* 2010, Woodhouse *et al* 2010, Pederson *et al* 2013, Cook *et al* 2016a, 2016b, Williams *et al* 2020), including studies that have found the recent pluvial to be the largest in at least 400–500 years in the Midwest and Northeast US (Pederson *et al* 2013, Ford 2014, Maxwell and Harley 2017). No studies, however, have contextualized the recent intensification of the aridity gradient. Here, we (a) evaluate and contextualize the spatial characteristics and physical mechanisms of the modern summer (JJA) aridity gradient within its natural range of climate variability using a tree-ring reconstruction of soil moisture anomalies over central North America, and (b) decompose the effects of observed and anthropogenic climate variability on the recent intensification of the aridity gradient. Through this analysis, we gain a better understanding of what mechanisms drive the aridity gradient outside of its natural range of variability, which is critical to disentangle how trends in natural low-frequency and anthropogenic climate change will impact future North American hydroclimate trends.

## 2. Materials and methods

### 2.1. Climate and soil moisture data

We used monthly  $1/4^\circ$  grids of 1901–2020 total precipitation (summed over all days), mean daily maximum ( $T_{\max}$ ) and minimum temperatures ( $T_{\min}$ ), relative humidity, wind speed, and solar and longwave radiation from a variety of climate data products. The methods used to develop these datasets are detailed in Williams *et al* (2017) and Williams *et al* (2020). Observations of long-term, spatially continuous soil moisture do not exist, so we incorporated an updated record of modeled gridded ( $1/4^\circ$ ) monthly 1901–2020 soil moisture anomalies from Williams *et al* (2020). The model was forced by the monthly climate data described above and calibrated to optimize agreement with monthly mean 0–200 cm soil moisture plus snow water equivalent as simulated by the Noah land-surface community model (Ek 2003). To avoid the effects of recent anthropogenic trends on baseline estimates, modeled soil moisture and climate data were standardized relative to 1910–1960 climatological means and variances.

### 2.2. Tree-ring reconstruction of summer soil moisture

We produced gridded ( $1^\circ$ ) summer (JJA) soil moisture reconstructions across central North America ( $24\text{--}50^\circ\text{N}$ ,  $66\text{--}130^\circ\text{W}$ ), which included the contiguous United States, northern Mexico and southeastern Canada, using a network of 2800 chronologies of tree-ring width index values standardized to preserve low-to-medium frequency variability (Melvin and

Briffa 2008), predominantly accessed from the International Tree-Ring Databank ([www.ncdc.noaa.gov/paleo/treering.html](http://www.ncdc.noaa.gov/paleo/treering.html)). The tree-ring dataset is an updated version of that used by Stahle *et al* (2020).

We reconstructed gridded records of standardized JJA 0–200 cm soil moisture anomalies (SMz) using the standard point-by-point nested reconstruction methods used to develop the North American Drought Atlas (Cook *et al* 1999, 2004, 2010). The SMz data are updated from Williams *et al* (2020). We produced our own gridded soil-moisture reconstruction rather than the North American Drought Atlas to facilitate comparisons to idealized soil-moisture calculations covering the observational interval described in sections 2.3 and 2.4. Following Williams *et al* (2020) and Williams *et al* (2021), we produced an ensemble of reconstructions using varying calibration periods (1901–1978, –1983, –1990, –2000), search radii (50, 100, 150, 200, 300, 400, 500 km), spatial smoothing (1, 3, 5 degrees smoothing), and minimum chronology length (1850–, 1800–, 1750–, 1700–, 1650–, 1600–1978). Reconstruction models were cross-validated using an iterative leave-a-decade out approach (see Williams *et al* 2020, Bolles *et al* 2021 for methods), correlating out-of-sample reconstruction time series against the target time series (cross-validated  $R^2$ ).

Following Williams *et al* (2021), alternate reconstructions then replaced the primary reconstruction (calibration period: 1901–1978, search radius: 150 km, spatial smoothing: 3 grid-cells, minimum chronology length: 1850–1978) when either (a) the corrected Akaike Information Criterion ( $AIC_C$ ; Akaike 1974) decreased by at least two without reducing the cross-validated  $R^2$  or reconstruction length, or (b) the reconstruction length increased by at least 10 years without reducing  $R^2$  or increasing  $AIC_C$ . Maps of the reconstruction parameters are provided in figure S1 (available online at [stacks.iop.org/ERL/16/114043/mmedia](https://stacks.iop.org/ERL/16/114043/mmedia)).

Regionally-averaged SMz reconstructions were calculated for eastern (eastern NA; 24–50°N, 66–100°W; eastern United States and southeastern Canada) and western North America (western NA; 24–50°N, 100–130°W; western United States and northern Mexico), omitting grid cells with  $R^2 < 0.2$ . The reconstructions were then bias-corrected to match the calibration period variance of the target time series, as variances of regionally-averaged reconstructed time series can shift due to changes in available tree-ring records (Williams *et al* 2020). Next, regional observed and reconstructed SMz time series were standardized to the 1400–1960 mean and variance (calculated after replacing reconstructed values with observations during 1901–2020). The ‘east-west North American aridity gradient’ was calculated as eastern minus western NA SMz and is referred to as the ‘aridity gradient’ for the remainder

of the paper. Positive aridity gradient values therefore represent years when SMz anomalies are more positive in eastern than in western NA and negative aridity gradient values represent the opposite. The location of the aridity gradient is dynamic and large historic shifts in the gradient’s background mean location could reduce temporal variability in our calculations of east-west aridity differences. However, under a strong radiative forcing scenario, Seager *et al* (2018b) found the location of the aridity gradient to shift by approximately 2° longitude, small relative to the sizes of our eastern and western NA study regions. It is thus unlikely that our reconstruction of the aridity gradient’s strength is strongly impacted by pre-observational shifts in the precise location of the east-west dividing line. Throughout the paper we focus on 20 year running means of regional SMz and the aridity gradient. The reasoning is that the 21st century has thus far been nearly continuously dry across much of western NA while, across much of the eastern NA, annual precipitation totals generally remained high following strong positive trends over the 20th century. As our observational climate data ended in 2020, this study focuses on 20 year running means specifically to compare the strong aridity gradient during 2001–2020 to all other observed and reconstructed 20 year periods.

### 2.3. Effects of observed climate variability on the aridity gradient

We considered the effects of observed variability in monthly precipitation, temperature, and relative humidity on the aridity gradient to account for the effects of evaporative demand and water limitations. We isolated the effect of potential evapotranspiration (PET; calculated as the Penman-Monteith reference evapotranspiration from  $T_{max}$ ,  $T_{min}$ , solar radiation, relative humidity, and wind) and then the combined effects of temperature and humidity within PET on SMz as the change in SMz caused by allowing the variable of interest to vary and holding remaining variables at mean 1910–1960 climatology (e.g. Williams *et al* 2015). The precipitation effect was then isolated as the portion of SMz not attributed to PET.

The same approach was used to isolate the contributions of climate variables during specific seasons (Spring MAM, Summer JJA, Fall SON, Winter DJF). This leads to eight counterfactual seasonal records, where each season is assigned a recalculated version of precipitation or temperature and humidity. Temperature and humidity work together to affect evaporative demand. Contributions of all climate forcing variables to SMz were nearly additive, but nonlinearities prevent the contributions from being perfectly so. Seasonal contributions were therefore rescaled to sum to 100% of each annual contribution and annual contributions were rescaled to sum to the total SMz time series.

## 2.4. Effects of anthropogenic climate trends on the aridity gradient

We characterized the effects of modeled anthropogenic climate trends on the aridity gradient as the difference between the observed aridity gradient and a counterfactual time series calculated with climate data after removing simulated anthropogenic trends. We characterized anthropogenic climate trends as the multi-model mean trends in precipitation, temperature, and humidity as simulated by 29 models that participated in the sixth phase of the Coupled Model Intercomparison Project (CMIP6) (Eyring *et al* 2016). Following Williams *et al* (2020), modeled trends were assessed as 50 year low-pass filtered time series of temperature and humidity and 100 year low-pass filtered precipitation totals from 1850 to 2100, where 1850–2014 data come from the CMIP6 Historical experiment and 2015–2100 data come from tier 1 of the shared socioeconomic pathway 2–4.5 (SSP2-4.5; medium-forcing pathway of  $+4.5 \text{ W m}^{-2}$ ) scenario from ScenarioMIP (O'Neill 2016). For precipitation, CMIP6 typically projects smaller anthropogenic trends relative to interdecadal variability, necessitating a longer filter. To reduce effects of outliers, monthly precipitation values were log-transformed prior to filtering. Next, low-pass filtered time series are converted to change since 1901. For precipitation, change since 1901 is calculated as fractional change (each month's filtered precipitation is divided by the filtered value in 1901). Time series of change since 1901 were then subtracted (divided for precipitation) away from the observed time series in order to calculate counterfactual realizations of the observed climate history absent of modeled climate trends. Modeled uncertainty in anthropogenic trends was characterized by the range of trends simulated among the 29 models. The 29 models considered were selected based on availability of monthly precipitation, temperatures, and relative humidity data for Historical and SSP2-4.5 experiments. This approach is described in detail in the supplementary materials of Williams *et al* (2020), although that study used CMIP5 simulations.

## 3. Results and discussion

### 3.1. Climate trends

During 1901–2020, 97% of eastern NA land area experienced positive precipitation trends (59% significant;  $p < 0.05$ ) while 45% of western NA experienced negative precipitation trends (3% significant) (figure 1(a)). For summer  $T_{\text{max}}$ , 37% of eastern NA experienced cooling (8% significant), while 96% of western NA warmed (82% significant) (figure 1(b)). These trends led to a positive trend in the aridity gradient since 1901, with 78% and 64% of eastern and western NA experiencing positive and negative SMz trends (31% and 18% significant), respectively (figure 1(c)). The divergence in eastern versus

western hydroclimatic trends has been particularly strong since the 1980s, leading to 2001–2020 being the largest 20 year period of positive aridity gradient in the observed record (figures 1(a)–(c)). These climate trends are consistent with numerous regional studies across North America (Seager *et al* 2012, Easterling 2017, Mascioli *et al* 2017, Williams *et al* 2017, 2020, Bishop *et al* 2019a, 2019b).

### 3.2. Tree-ring reconstruction of aridity gradient

The observed aridity gradient has a consistent east-west contrast in correlations with tree-ring width records across North America (figure 2(a)). This indicates the tree-ring network's potential to contextualize the recent strengthening of the aridity gradient. Reconstructions of gridded SMz were generally more skillful in the West than in the East and many grid cells in the Northeast and Midwest were disqualified ( $R^2 < 0.2$ ) (figure 2(b)). However, the gridded SMz reconstruction still overlaps with 85% of eastern NA land area that experienced 1901–2020 soil moisture increases (figure S2). Reconstructed western and eastern NA SMz ( $R^2 = 0.79$  and  $0.67$ , respectively) and the aridity gradient ( $R^2 = 0.68$ ) were skillful back to 1400 CE (figure 2(c)).

We evaluated 20 year running means of reconstructions and observations of western NA SMz, eastern NA SMz, and the aridity gradient to contextualize the 2001–2020 extreme aridity gradient relative to the past six centuries. In western NA, there were four distinct multi-decade pluvial events during the early- and late-20th, early-17th, and mid-to-late 16th centuries, and three multi-decade drought events in the late-19th, late-16th to early-17th, and early-21st centuries (figure 2(d)). In eastern NA, multi-decadal variability was generally less pronounced than in the West, consistent with Herweijer *et al* (2007). The largest multi-decade swings in the east consisted of long-term drying in the mid-to-late 1500s, wetting in the late 1500s to early 1600s, and wetting in the 20th and early-21st centuries (figure 2(e)). Opposing SMz trends in eastern and western NA led to distinct peaks in the aridity gradient reconstruction, and the strongest positive (wet east, dry west) gradients occurred in 2001–2020, 1574–1593, and 1846–1865 (ordered from most to least positive). The strongest negative gradients (dry east, wet west) occurred in 1976–1995, 1549–1568, and 1906–1925 (ordered from most to least negative) (figure 2(f)). The latter period includes the noted North American pluvial centered in the west (Fye *et al* 2003, Woodhouse *et al* 2005, Cook *et al* 2011). Over the past few decades, the swing from the most negative aridity gradient of  $-0.91 \sigma$  in 1976–1995 to the most positive mean aridity gradient of  $+1.00 \sigma$  in 2001–2020 resulted in the most rapid aridity gradient reversal since 1400 CE ( $\Delta = +1.91 \sigma$ ). This reversal was rivaled only by the late-1500s reversal ( $\Delta = +1.52 \sigma$ ) from  $-0.73 \sigma$  in 1549–1568 to  $+0.79 \sigma$  in 1574–1593.

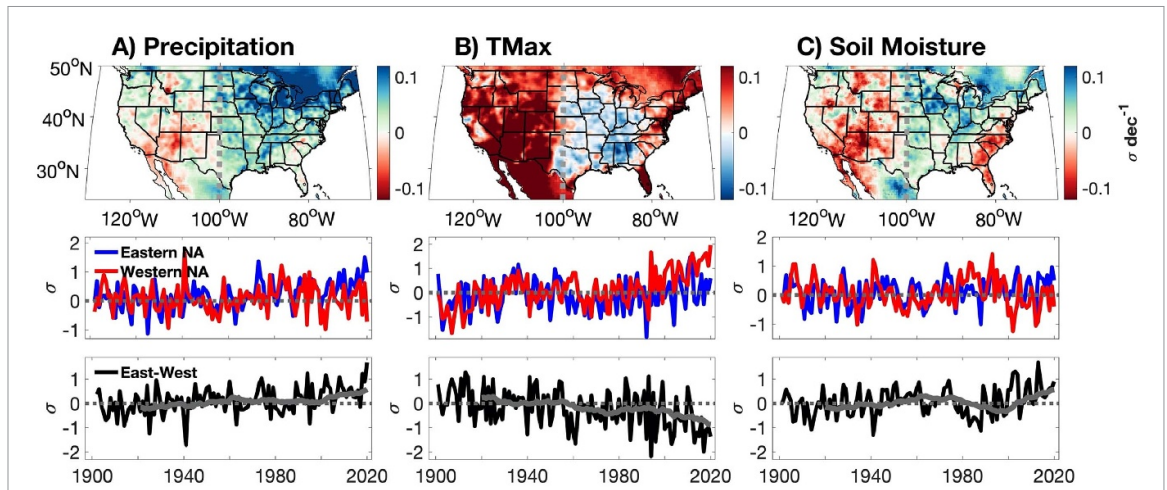


**Figure 1.** 1901–2020 standardized climate trends (top), regionally-averaged eastern ( $<100^\circ\text{W}$ ; eastern NA) and western North America ( $>100^\circ\text{W}$ ; western NA) time series (middle), and eastern minus western NA difference (east-west; bottom) in (a) Climgrid water year (prior year October—current year September) precipitation totals, (b) Climgrid summer (June—August) mean daily maximum temperature, and (c) Noah land-surface model-calibrated 0–200 cm summer soil moisture fraction. Dashed grey line in top panels:  $100^\circ\text{W}$ . Grey line in bottom panels: 20 year running mean assigned to final year in each 20 year window.

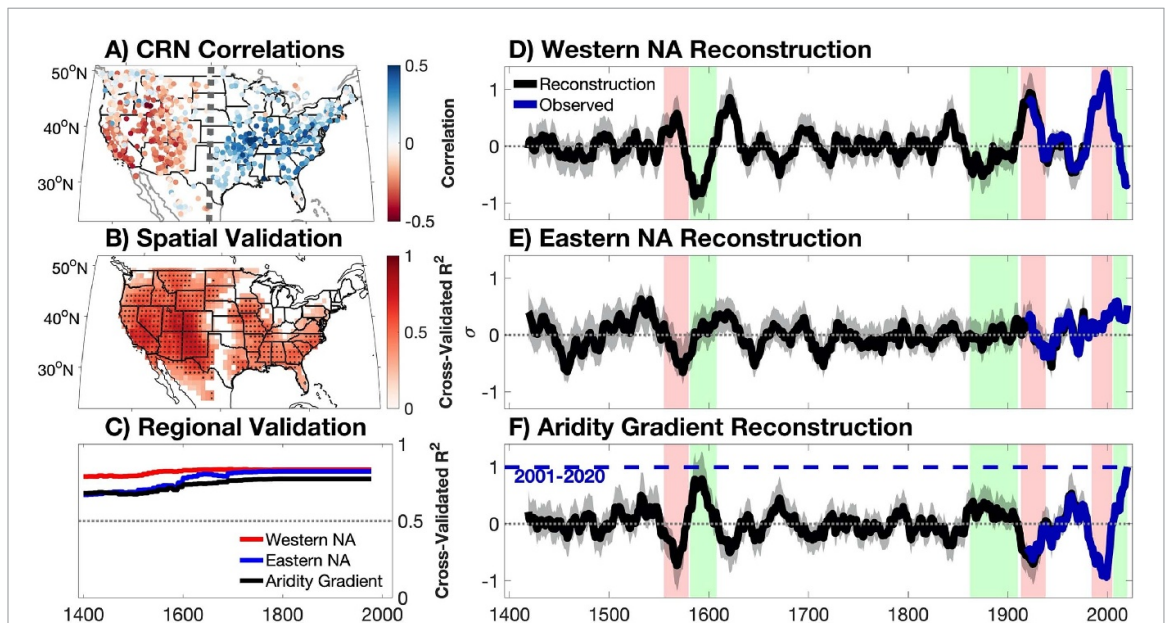
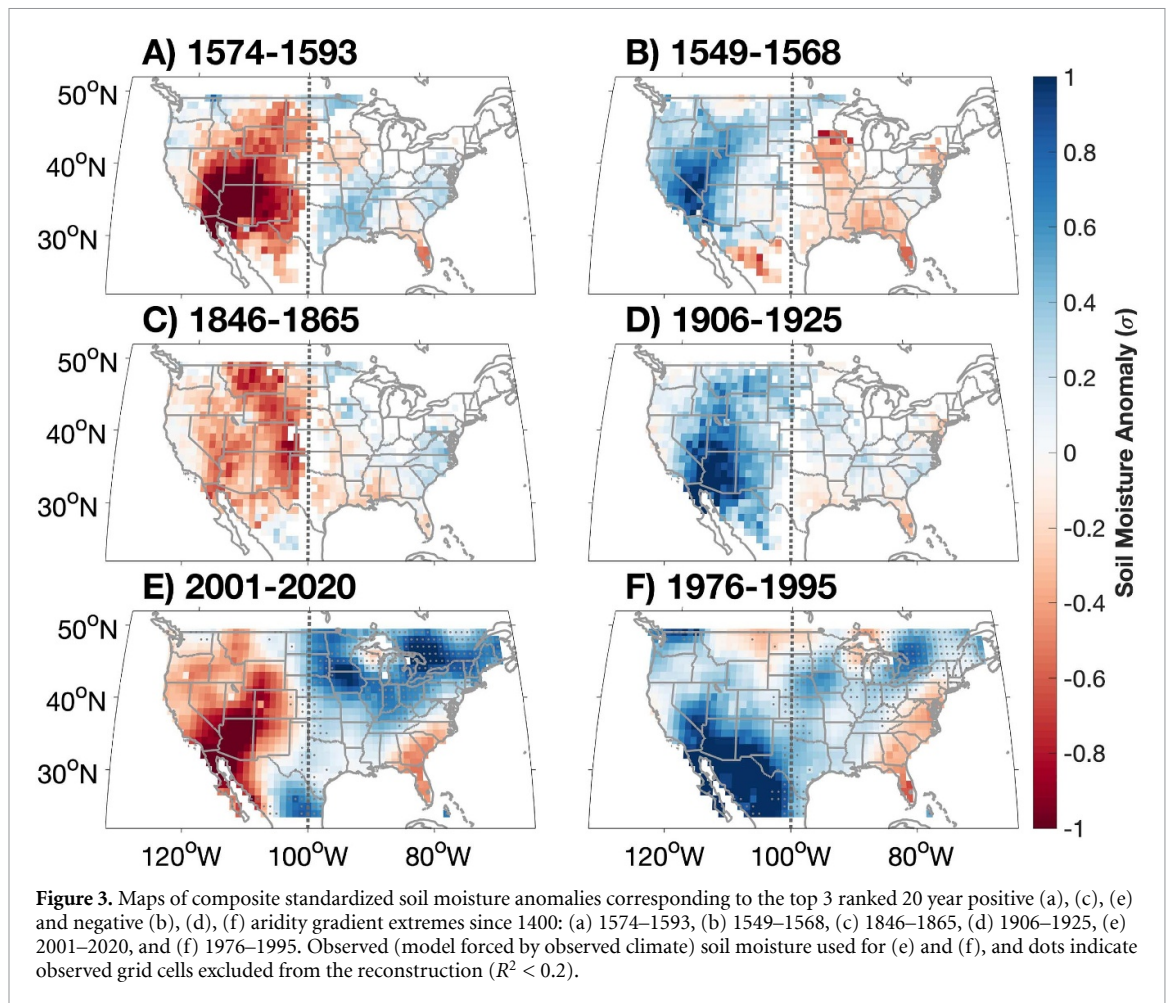


**Figure 2.** Summer east-west North American aridity gradient reconstruction. (a) Correlation between observed 1901–1978 observed aridity gradient and North American tree-ring network chronologies (CRN); (b) cross-validated reconstruction skill of gridded soil moisture reconstructions ( $R^2$ ; black dots:  $R^2 \geq 0.4$ ; white:  $R^2 < 0.2$  or reconstruction does not extend to 1400 CE); (c) time-resolved cross-validated  $R^2$  of reconstructions of the aridity gradient (black) and regionally averaged standardized anomalies of soil moisture in eastern (blue) and western (red) North America; and time series of reconstructed (black) and observed (blue) 20 year running-mean standardized anomalies of (d) western and (e) eastern North America soil moisture and (f) the aridity gradient. Gray shading in (d)–(f): 95% reconstruction confidence interval (see Williams *et al* 2020 for methods); pink and green shading in (d)–(f): most negative and positive aridity gradient extremes; blue dotted line in (f): 2001–2020 mean; running-mean values in (d)–(f) are assigned to the final year in each 20 year window.

The 2001–2020 aridity gradient remained the most positive when we retained all gridded soil moisture reconstructions (including  $R^2 < 0.2$ ; figure S3). We repeated the reconstruction over longer and shorter time frames, finding the magnitude of the 2001–2020 positive aridity gradient is highest for the shortest reconstructions, as these reconstructions represent more of eastern NA that experienced 20th-century wetting and exclude

higher-amplitude hydroclimatic swings of the Medieval period (figure S4).

The second-most positive aridity gradient in our reconstruction (1574–1593) coincided with the well-documented late-16th century megadrought in western North America (Stahle 2000, Cook *et al* 2018, Williams *et al* 2020) although the East was not as anomalously wet relative to 2001–2020 (figure 3(a)). Interestingly, the late 16th-century



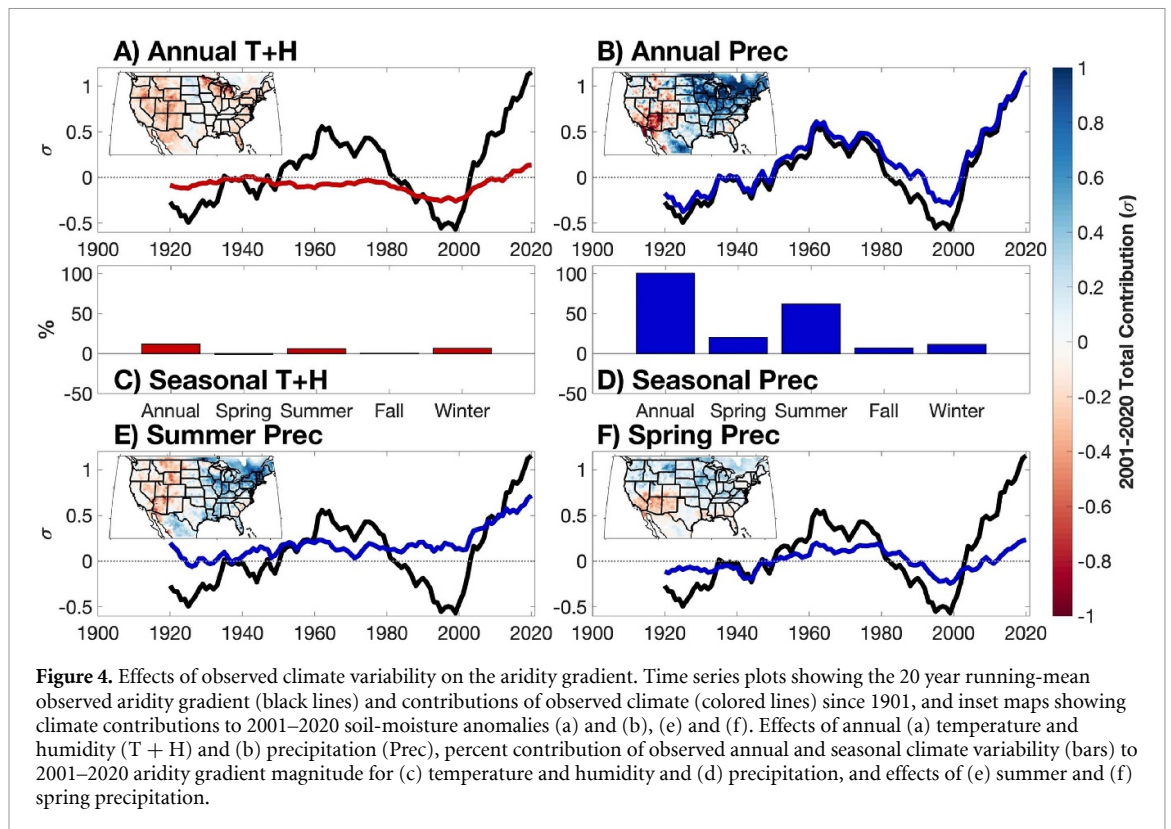
positive gradient immediately followed the second-most extreme negative aridity gradient in the reconstruction (1549–1568), similar to the record-breaking swing from 1976–1995 to 2001–2020 (figure 2(f)). But in the case of 1549–1568, the negative gradient was dominated by dry conditions in the eastern Great Plains (figure 3(b)). The third-highest positive and negative aridity gradients respectively occurred in the mid-19th and early-20th centuries. These events were promoted by the mid-19th century Civil War drought in the West (Herweijer *et al* 2006, 2007) and one of the wettest periods in the West on record (Fye *et al* 2003, Woodhouse *et al* 2005, Cook *et al* 2011), respectively (figures 3(c) and (d)). The most extreme aridity gradient magnitudes were influenced by the Southwest drought and the Midwest and Northern Plains pluvial during 2001–2020 and a late-20th century Southwest pluvial during 1976–1995 (figures 3(e) and (f)).

### 3.3. Effects of observed and anthropogenic climate trends

The observed precipitation increase in the Midwest and Northeast was the main driver of the 2001–2020 aridity gradient extreme. Annual temperature and humidity (T + H), primarily in western NA, positively forced the aridity gradient (+12%

effect relative to 2001–2020 aridity gradient magnitude) (figure 4(a)), but the annual precipitation forcing (+100%), mostly driven by positive eastern NA precipitation anomalies, accounted for the vast majority of the 2001–2020 aridity gradient anomaly (figure 4(b)). Given the strong negative SMz anomalies observed in the Southwest, we expected stronger roles for T + H on the 2001–2020 aridity gradient. The drying effects of T + H in the Midwest, however, dampened the effects of these variables on the aridity gradient while the drying effects of precipitation in the Southwest strengthened the aridity gradient (figures 4(a) and (b)). The >100% forcing from precipitation and T + H on the 2001–2020 aridity gradient was balanced by a –12% forcing from wind and solar radiation. While the T + H forcing was most positive during winter (+7%), the precipitation forcing was most positive during summer (+62%) and spring (+20%) (figures 4(c) and (d)), with weaker forcings (<11%) from the remaining seasonal contributions. The summer precipitation forcing resulted from long-term wetting in the Midwest and Northeast and some recent drying across the intermountain West (figure 4(e)).

Turning to the 1976–1995 negative aridity gradient, it received more balanced forcings from both annual T + H (–51%) and precipitation anomalies



(−42%) (figures 4(a) and (b)), predominantly from above-average spring and winter precipitation across the West and negative spring T + H forcings in the Midwest, suggesting that climate anomalies in the West were more important in promoting the negative aridity gradient extreme of 1976–1995 than the positive extreme of 2001–2020. While both observed and reconstructed aridity gradient indices suggest SMz variability in the western NA was the primary driver of past aridity gradient extremes, the recent positive aridity gradient extreme was principally driven by a century-long increase in eastern precipitation.

The contribution of anthropogenic climate change was confounded by high inter-model uncertainty. CMIP6 ensemble-mean anthropogenic precipitation trends were simulated to account for 15% of the observed 2001–2020 aridity gradient anomaly, which was counteracted by a slight negative forcing of −2% from anthropogenic trends in T + H (figure 5(a)). That is, the multi-model mean precipitation increases positively forced SMz in the East more than in the West. Notably, there was considerable inter-model spread in the contribution of anthropogenic precipitation trends to the aridity gradient (figures 5(b) and (d)). Modeled effects of anthropogenic T + H trends were more consistent, with all models simulating a warming-driven drying effect across the study domain and 52% of models indicating a negative effect on the historical aridity gradient (figures 5(c) and (e)).

The above results imply a large degree of uncertainty in the effect of anthropogenic climate trends

on the aridity gradient to date. First, individual models exhibited a wide range of variability in terms of how anthropogenic climate change affects regional precipitation trends. Second, models consistently simulated more ubiquitous warming across North America than was observed. Both could indicate that the effect of anthropogenic climate trends on the aridity gradient are not accurately represented by CMIP6 climate models. It is also plausible, however, that the multi-model mean is an accurate representation of anthropogenic forcing and that the recent intensification of the aridity gradient was dominated by internal climate variability. Resolving uncertainties in modeled regional anthropogenic climate trends, especially precipitation trends, will be critical to understand the future evolution of the aridity gradient, improve annual-to-decadal prediction of regional-to-continental hydroclimate variability, and prepare the agricultural industry for shifts in soil moisture gradients over North America.

Last, to evaluate the impacts of atmospheric dynamics on aridity gradient variability, we calculated regional SMz and aridity gradient correlations with 1948–2020 National Center for Environmental Prediction and National Center for Atmospheric Research Reanalysis monthly 200 hPa geopotential height and skin temperature data (Kalnay 1996). Positive aridity gradients were associated with a winter-spring atmospheric wave train that sheltered the western NA from Pacific storms, likely linked to cool eastern tropical Pacific sea surface temperatures (figure 6). It is well-documented that 21st century



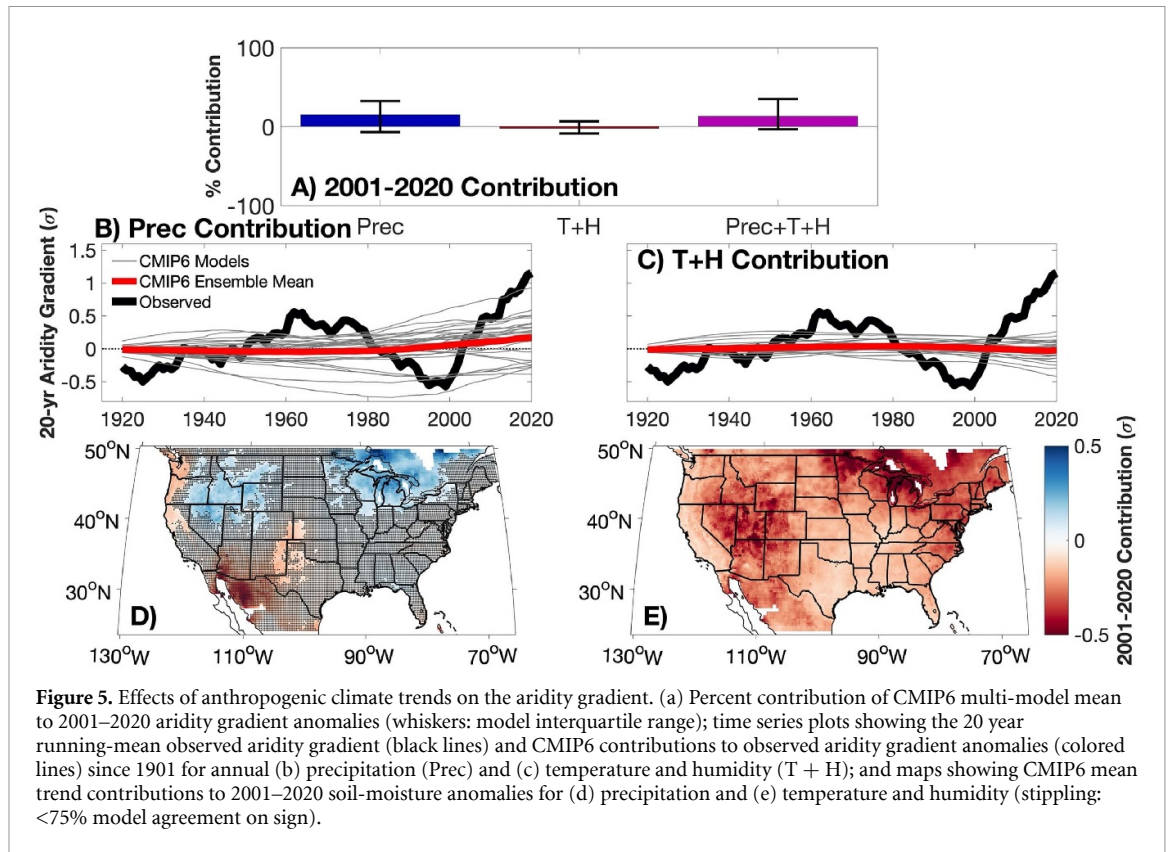


**Figure 5.** Effects of anthropogenic climate trends on the aridity gradient. (a) Percent contribution of CMIP6 multi-model mean to 2001–2020 aridity gradient anomalies (whiskers: model interquartile range); time series plots showing the 20 year running-mean observed aridity gradient (black lines) and CMIP6 contributions to observed aridity gradient anomalies (colored lines) since 1901 for annual (b) precipitation (Prec) and (c) temperature and humidity (T + H); and maps showing CMIP6 mean trend contributions to 2001–2020 soil-moisture anomalies for (d) precipitation and (e) temperature and humidity (stippling: <75% model agreement on sign).

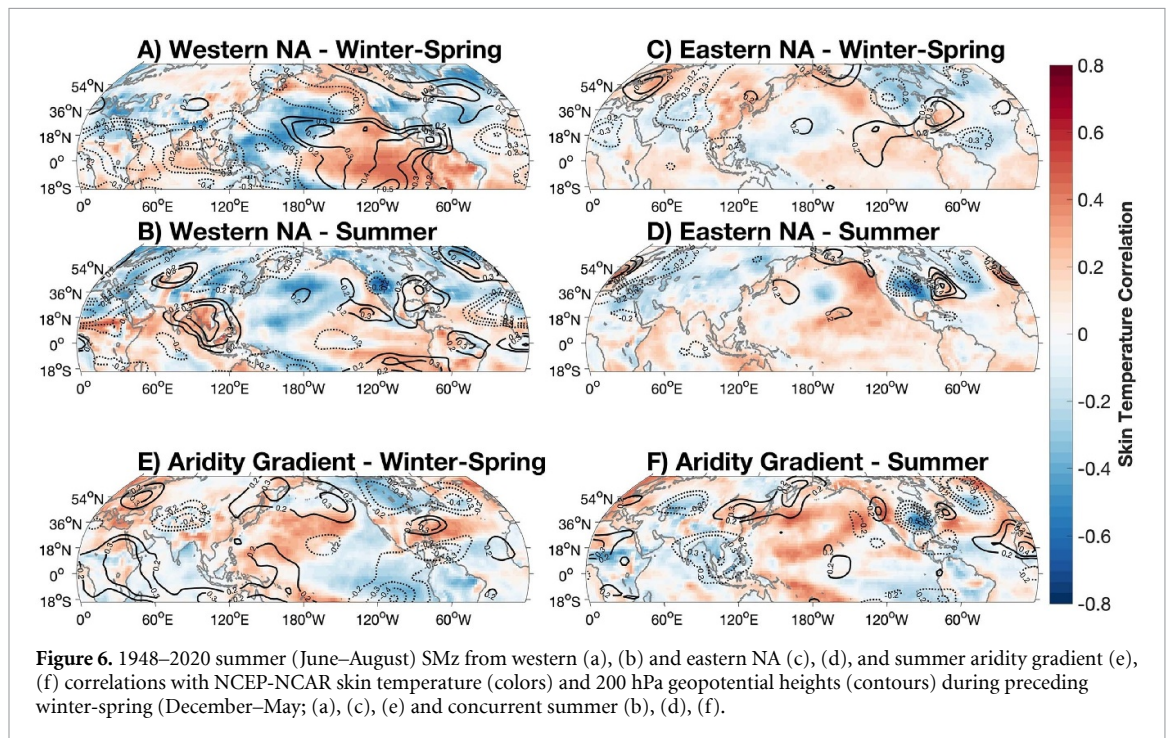


**Figure 6.** 1948–2020 summer (June–August) SMz from western (a), (b) and eastern NA (c), (d), and summer aridity gradient (e), (f) correlations with NCEP-NCAR skin temperature (colors) and 200 hPa geopotential heights (contours) during preceding winter-spring (December–May; (a), (c), (e) and concurrent summer (b), (d), (f).

drought conditions in western NA were associated with anomalously cool conditions in the tropical Pacific (Delworth *et al* 2015, Lehner *et al* 2018) and that similar conditions were likely responsible for some or all of the reconstructed western North American megadroughts of the last millennium (Seager *et al* 2007a, 2015, Huang and Xie 2015, Cook *et al* 2018, Steiger *et al* 2019, 2021).

While western hydroclimatic variability was the dominant driver of decadal variability in the aridity gradient over the past 400 years, the exceptional 2001–2020 aridity gradient magnitude was exacerbated by increased summer precipitation in eastern NA. During the summer months, positive aridity gradients were associated with a midlatitude wave train over North America, which likely promoted

increased storm track activity in the Great Plains and Southeast (figure 6). While past studies have dynamically linked eastern precipitation variability to the NASH and the Great Plains Low-Level Jet providing enhanced moisture transport from the Gulf of Mexico into eastern North America (Weaver and Nigam 2008, Seager *et al* 2012, Bishop *et al* 2019a), the results here do not establish a link between the NASH and the summer aridity gradient. Further research into recent trends in both Pacific and Atlantic teleconnections with North American hydroclimate will be needed to establish dynamic causes and accurately project future changes in this phenomenon, especially the long-term eastern precipitation trend. This work motivates further work to understand land-atmosphere interactions and the degree to which regional soil-moisture trends, or trends in soil-moisture gradients, may feedback to affect climate at regional-to-continental scales (e.g. Seneviratne *et al* 2010, Koster *et al* 2016).

#### 4. Conclusions

Our tree-ring reconstructions of North American summer soil moisture anomalies provide a robust estimate of how the east-west North American aridity gradient has varied over the past six centuries and demonstrates that the 2001–2020 aridity gradient was very likely the most extreme 20 year gradient since at least 1400 CE. These reconstructions introduce a novel conceptual model for hydroclimate variability that could improve predictions of spatial and temporal variability in North American drought and floods. In the reconstruction, previous inter-decadal variations in the aridity gradient closely followed western North American soil moisture variability, but the extreme gradient observed in recent decades, and ongoing as of fall 2021, was largely driven by a century-long increase in eastern North American soil moisture. The ongoing extreme positive aridity gradient was immediately preceded by the most negative extreme gradient in the reconstructed record, making the transition from negative to positive decadal aridity gradient anomalies the most rapid in over 600 years. The 2001–2020 aridity gradient was largely driven by precipitation increases in eastern North America, particularly in summer, with minor additional effects from recent temperature and humidity increases and spring precipitation decreases in western North America. CMIP6 simulations suggest that anthropogenic climate trends were not major contributors to the 2001–2020 aridity gradient, though interpretation of anthropogenic climate effects is confounded by inter-model disagreement among regional anthropogenic precipitation trends and disagreement between observed and simulated temperature and humidity trends in the East.

Recent and potentially ongoing trends toward drying in western North America and wetting

in eastern North America, and notable disagreements between observed hydroclimatic trends and those simulated by climate models to arise from anthropogenic forcing, especially in the East, underscore a concerning uncertainty in how human and natural systems will be impacted by changes in water supply through the 21st century (e.g. Frei *et al* 2002, Luce *et al* 2012, Pederson *et al* 2013). The fluctuating strength of the east-west North American aridity gradient has been a natural, multi-decadal mode of hydroclimate variability across North America for centuries (Woodhouse *et al* 2009) but its evolution and impacts through the late-21st century remain uncertain. Further research will be needed to identify the aridity gradient effects of large-scale circulation on pan-continental soil moisture gradients, the degree to which the east and west trends are dynamically related, and how the aridity gradient affects North American climate via land-atmosphere interactions. In addition to changes in the aridity gradient, models project aridification and a reduction in surface water availability across much of the continent largely due to warming (Mankin *et al* 2017, 2018, Seager *et al* 2018b), which could alter the strength and extent of the aridity gradient in the coming decades. The water resources and food security of tens of millions will be impacted by the hydroclimate trends investigated here, escalating the need to resolve the causes of and future changes in regional moisture availability.

#### Data availability statement

The data that support the findings of this study are available upon reasonable request from the authors.

#### Acknowledgments

This research was supported by the NASA Earth and Space Science Graduate Student Fellowship (80NSSC17K0402), the National Science Foundation (AGS-1703029 and AGS-1401400), and NOAA award NA17OAR4310126. MPR was supported by the NOAA Climate and Global Change Postdoctoral Fellowship Program, administered by UCAR's Cooperative Programs for the Advancement of Earth System Science (CPAESS) under Award #NA18NWS4620043B.

#### ORCID iDs

Daniel A Bishop  <https://orcid.org/0000-0002-0394-5996>

A Park Williams  <https://orcid.org/0000-0001-8176-8166>

Richard Seager  <https://orcid.org/0000-0003-4772-9707>

Edward R Cook  <https://orcid.org/0000-0001-7478-4176>

Dorothy M Peteet  <https://orcid.org/0000-0003-3029-7506>  
 Benjamin I Cook  <https://orcid.org/0000-0002-4501-9229>  
 Mukund P Rao  <https://orcid.org/0000-0003-3398-2453>  
 David W Stahle  <https://orcid.org/0000-0002-8943-2541>

## References

- Akaike H 1974 A new look at the statistical model identification *IEEE Trans. Autom. Control* **19** 716–23
- Baker R G, Bettis E A III, Denniston R F, Gonzalez L A, Strickland L E and Krieg J R 2002 Holocene paleoenvironments in southeastern Minnesota—chasing the prairie-forest ecotone *Palaeogeogr. Palaeoclimatol. Palaeoecol.* **177** 103–22
- Barandiaran D, Wang S-Y and Hilburn K 2013 Observed trends in the Great Plains low-level jet and associated precipitation changes in relation to recent droughts *Geophys. Res. Lett.* **40** 6247–51
- Bishop D A, Williams A P and Seager R 2019b Increased fall precipitation in the southeastern United States driven by higher-intensity, frontal precipitation *Geophys. Res. Lett.* **46** 8300–9
- Bishop D A, Williams A P, Seager R, Fiore A M, Cook B I, Mankin J S, Singh D, Smerdon J E and Rao M P 2019a Investigating the causes of increased twentieth-century fall precipitation over the southeastern United States *J. Clim.* **32** 575–90
- Bolles K C, Williams A P, Cook E R, Cook B I and Bishop D A 2021 Tree-ring reconstruction of the atmospheric ridging feature that causes flash drought in the central United States since 1500 *Geophys. Res. Lett.* **48** e2020GL091271
- Cook B I, Anchukaitis K J, Touchan R, Meko D M and Cook E R 2016a Spatiotemporal drought variability in the Mediterranean over the last 900 years *J. Geophys. Res. Atmos.* **121** 2060–74
- Cook B I, Ault T R and Smerdon J E 2015 Unprecedented 21st century drought risk in the American Southwest and Central plains *Sci. Adv.* **1** e1400082
- Cook B I, Cook E R, Smerdon J E, Seager R, Williams A P, Coats S, Stahle D W and Diaz J V 2016b North American megadroughts in the common Era: reconstructions and simulations *Wiley Interdiscip. Rev. Clim. Change* **7** 411–32
- Cook B I, Mankin J S, Marvel K, Williams A P, Smerdon J E and Anchukaitis K J 2020 Twenty-first century drought projections in the CMIP6 forcing scenarios *Earth's Future* **8** e2019EF001461
- Cook B I, Seager R and Miller R L 2011 On the causes and dynamics of the early twentieth-century North American pluvial *J. Clim.* **24** 5043–60
- Cook B I, Smerdon J E, Seager R and Coats S 2014 Global warming and 21st century drying *Clim. Dyn.* **43**(9) 2607–27
- Cook B I, Williams A P, Smerdon J E, Palmer J G, Cook E R, Stahle D W and Coats S 2018 Cold tropical Pacific sea surface temperatures during the late sixteenth-century North American megadrought *J. Geophys. Res. Atmos.* **123** 11,307–11,320.
- Cook E R, Meko D M, Stahle D W and Cleaveland M K 1999 Drought reconstructions for the continental United States *J. Clim.* **12** 1145–62
- Cook E R, Seager R, Heim R R, Vose R S, Herweijer C and Woodhouse C 2010 Megadroughts in North America: placing IPCC projections of hydroclimatic change in a long-term palaeoclimate context *J. Quat. Sci.* **25** 48–61
- Cook E R, Woodhouse C A, Eakin C M, Meko D M and Stahle D W 2004 Long-term aridity changes in the western United States *Science* **306** 1015–8
- Delworth T L, Zeng F, Rosati A, Vecchi G A and Wittenberg A T 2015 A link between the hiatus in global warming and North American drought *J. Clim.* **28** 3834–45
- Easterling D Coauthors 2017 Precipitation change in the United States *Climate Science Special Report: Fourth National Climate Assessment* Vol I, ed D J Wuebbles Coauthors (Washington DC, USA: U.S. Global Change Research Program) pp 207–30
- Ek M B Coauthors 2003 Implementation of Noah land surface model advances in the National Centers for environmental prediction operational mesoscale Eta model *J. Geophys. Res. Atmos.* **108**
- Eyring V, Bony S, Meehl G A, Senior C, Stevens B, Stouffer R J and Taylor K E 2016 Overview of the Coupled Model Intercomparison Project Phase 6 (CMIP6) experimental design and organisation *Geosci. Model Dev. Discuss.* **8** 1937–58
- Ford T W 2014 Precipitation anomalies in eastern-Central Iowa from 1640–present *J. Hydrol.* **519** 918–24
- Frei A, Armstrong R L, Clark M P and Serreze M C 2002 Catskill Mountain water resources: vulnerability, hydroclimatology, and climate-change sensitivity *Ann. Assoc. Am. Geogr.* **92** 203–24
- Fye F K, Stahle D W and Cook E R 2003 Paleoclimatic analogs to twentieth-century moisture regimes across the United States *Bull. Am. Meteorol. Soc.* **84** 901–10
- Gensini V A and Brooks H E 2018 Spatial trends in United States tornado frequency *npj Clim. Atmos. Sci.* **1** 1–5
- Hartmann D L Coauthors 2013 Observations: atmosphere and surface *Climate Change 2013: The Physical Science Basis: Working Group I Contribution to the Fifth Assessment Report of the Intergovernmental Panel on Climate Change* ed T F Stocker Coauthors (Cambridge: Cambridge University) pp 159–254
- Herrera-Estrada J E, Martinez J A, Dominguez F, Findell K L, Wood E F and Sheffield J 2019 Reduced moisture transport linked to drought propagation across North America *Geophys. Res. Lett.* **46** 5243–53
- Herweijer C, Seager R and Cook E R 2006 North American droughts of the mid to late nineteenth century: a history, simulation and implication for Mediaeval drought *Holocene* **16** 159–71
- Herweijer C, Seager R, Cook E R and Emile-Geay J 2007 North American droughts of the last millennium from a gridded network of tree-ring data *J. Clim.* **20** 1353–76
- Huang P and Xie S P 2015 Mechanisms of change in ENSO-induced tropical Pacific rainfall variability in a warming climate *Nat. Geosci.* **8** 922–6
- Kalnay E Coauthors 1996 The NCEP/NCAR 40-year reanalysis project *Bull. Am. Meteorol. Soc.* **77** 437–71
- Koster R D, Chang Y, Wang H and Schubert S D 2016 Impacts of local soil moisture anomalies on the atmospheric circulation and on remote surface meteorological fields during boreal summer: a comprehensive analysis over North America *J. Clim.* **29** 7345–64
- Lanici J M, Carlson T N and Warner T T 1987 Sensitivity of the Great Plains severe-storm environment to soil-moisture distribution *Mon. Weather Rev.* **115** 2660–73
- Lehner F, Deser C, Simpson I R and Terray L 2018 Attributing the U.S. Southwest's recent shift into drier conditions *Geophys. Res. Lett.* **45** 6251–61
- Leibensperger E M Coauthors 2012 Climatic effects of 1950–2050 changes in US anthropogenic aerosols—part 2: climate response *Atmos. Chem. Phys.* **12** 3349–62
- Li L, Li W and Kushnir Y 2012 Variation of the North Atlantic subtropical high western ridge and its implication to Southeastern US summer precipitation *Clim. Dyn.* **39** 1401–12
- Luce C H, Vose J M, Pederson N, Campbell J, Millar C, Kormos P and Woods R 2012 Contributing factors for drought in United States forest ecosystems under projected future climates and their uncertainty *For. Ecol. Manage.* **380** 299–308

- Mankin J S, Seager R, Smerdon J E, Cook B I, Williams A P and Horton R M 2018 Blue water trade-offs with vegetation in a CO<sub>2</sub>-enriched climate *Geophys. Res. Lett.* **45** 3115–25
- Mankin J S, Smerdon J E, Cook B I, Williams A P and Seager R 2017 The curious case of projected 21st-century drying but greening in the American West *J. Clim.* **30** 8689–710
- Mascioli N R, Previdi M, Fiore A M and Ting M 2017 Timing and seasonality of the United States ‘warming hole’ *Environ. Res. Lett.* **12** 034008
- Maxwell J T and Harley G L 2017 Increased tree-ring network density reveals more precise estimations of sub-regional hydroclimate variability and climate dynamics in the Midwest, USA *Clim. Dyn.* **49** 1479–93
- Melvin T M and Briffa K R 2008 A “signal-free” approach to dendroclimatic standardisation *Dendrochronologia* **26** 71–86
- Mueller N D, Butler E E, McKinnon K A, Rhines A, Tingley M, Holbrook N M and Huybers P 2016 Cooling of US Midwest summer temperature extremes from cropland intensification *Nat. Clim. Change* **6** 317–22
- Nikiel C A and Eltahir E A B 2019 Summer climate change in the midwest and great plains due to agricultural development during the twentieth century *J. Clim.* **32** 5583–99
- O’Neill B C Coauthors 2016 The scenario model intercomparison project (ScenarioMIP) for CMIP6 *Geosci. Model Dev.* **9** 3461–82
- Pal J S and Eltahir E A B 2003 A feedback mechanism between soil-moisture distribution and storm tracks *Q. J. R. Meteorolog. Soc.* **129** 2279–97
- Pan Z, Arritt R W, Takle E S, Gutowski W J, Anderson C J and Segal M 2004 Altered hydrologic feedback in a warming climate introduces a “warming hole” *Geophys. Res. Lett.* **31** L17109
- Partridge T F Coauthors 2018 Spatially distinct seasonal patterns and forcings of the U.S. warming hole *Geophys. Res. Lett.* **45** 2055–63
- Pederson N, Bell A R, Cook E R, Lall U, Devineni N, Seager R, Eggleston K and Vranes K P 2013 Is an epic pluvial masking the water insecurity of the greater New York City region? *J. Clim.* **26** 1339–54
- Portmann R W, Solomon S and Hegerl G C 2009 Spatial and seasonal patterns in climate change, temperatures, and precipitation across the United States *Proc. Natl Acad. Sci.* **106** 7324–9
- Seager R Coauthors 2007b Model projections of an imminent transition to a more arid climate in southwestern North America *Science* **316** 1181–4
- Seager R, Feldman J, Lis N, Ting M, Williams A P, Nakamura J, Liu H and Henderson N 2018a Whither the 100th meridian? The once and future physical and human geography of America’s arid–humid divide. Part I: the story so far *Earth Interact.* **22** 1–22
- Seager R, Feldman J, Lis N, Ting M, Williams A P, Nakamura J, Liu H and Henderson N 2018b Whither the 100th meridian? The once and future physical and human geography of America’s arid–humid divide. Part II: the meridian moves east *Earth Interact.* **22** 1–24
- Seager R, Graham N, Herweijer C, Gordon A L, Kushnir Y and Cook E R 2007a Blueprints for Medieval hydroclimate *Quat. Sci. Rev.* **26** 2322–36
- Seager R, Hoerling M, Schubert S, Wang H, Lyon B, Kumar A, Nakamura J and Henderson N 2015 Causes of the 2011–14 California drought *J. Clim.* **28** 6997–7024
- Seager R, Pederson N, Kushnir Y, Nakamura J and Jurburg S 2012 The 1960s drought and the subsequent shift to a wetter climate in the Catskill Mountains region of the New York City watershed *J. Clim.* **25** 6721–42
- Seneviratne S I, Corti T, Davin E L, Hirschi M, Jaeger E B, Lehner I, Orlowsky B and Teuling A J 2010 Investigating soil moisture–climate interactions in a changing climate: a review *Earth Sci. Rev.* **99** 125–61
- Singh D, Tsiang M, Rajaratnam B and Diffenbaugh N S 2013 Precipitation extremes over the continental United States in a transient, high-resolution, ensemble climate model experiment *J. Geophys. Res. Atmos.* **118** 7063–86
- Stahle D W et al 2020 Dynamics, variability, and change in seasonal precipitation reconstructions for North America *J. Clim.* **33** 3173–95
- Stahle D W Coauthors 2000 Tree-ring data document 16th century megadrought over North America *EOS Trans. Am. Geophys. Union* **81** 121–5
- Steiger N J, Smerdon J E, Cook B I, Seager R, Williams A P and Cook E R 2019 Oceanic and radiative forcing of medieval megadroughts in the American Southwest *Sci. Adv.* **5** eaax0087
- Steiger N J, Smerdon J E, Seager R, Williams A P and Varuolo-Clarke A M 2021 ENSO-driven coupled megadroughts in north and south america over the last millennium *Nat. Geosci.* **14** 739–44
- Touchan R, Anchukaitis K J, Meko D M, Attalah S, Baisan C and Aloui A 2008 Long term context for recent drought in northwestern Africa *Geophys. Res. Lett.* **35**
- Wang Q Coauthors 2014 Temporal-spatial characteristics of severe drought events and their impact on agriculture on a global scale *Quat. Int.* **349** 10–21
- Weaver S J and Nigam S 2008 Variability of the Great Plains low-level jet: large-scale circulation context and hydroclimate impacts *J. Clim.* **21** 1532–51
- Webb T III, Cushing E J and Wright H E Jr 1983 Holocene changes in the vegetation of the Midwest *Late-quaternary Environments of the United States* vol 2 (Minneapolis, MN: University of Minnesota Press) pp 142–65
- Williams A P, Anchukaitis K J, Woodhouse C A, Meko B M, Cook B I, Bolles K and Cook E R 2021 Tree rings and observations suggest no stable cycles in Sierra Nevada cool-season precipitation *Water Resour. Res.* **57** e2020WR028599
- Williams A P Coauthors 2013 Temperature as a potent driver of regional forest drought stress and tree mortality *Nat. Clim. Change* **3** 292–7
- Williams A P, Cook B I, Smerdon J E, Bishop D A, Seager R and Mankin J S 2017 The 2016 southeastern U.S. drought: an extreme departure from centennial wetting and cooling *J. Geophys. Res. Atmos.* **122** 10888–905
- Williams A P, Cook E R, Smerdon J E, Cook B I, Abatzoglou J T, Bolles K, Baek S H, Badger A M and Livneh B 2020 Large contribution from anthropogenic warming to an emerging North American megadrought *Science* **368** 314–8
- Williams A P, Seager R, Abatzoglou J T, Cook B I, Smerdon J E and Cook E R 2015 Contribution of anthropogenic warming to California drought during 2012–2014 *Geophys. Res. Lett.* **42** 2015GL064924
- Woodhouse C A, Kunkel K E, Easterling D R and Cook E R 2005 The twentieth-century pluvial in the western United States *Geophys. Res. Lett.* **32**
- Woodhouse C A, Meko D M, MacDonald G M, Stahle D W and Cook E R 2010 A 1200-year perspective of 21st century drought in southwestern North America *Proc. Natl Acad. Sci.* **107** 21283–88
- Woodhouse C A, Russell J L and Cook E R 2009 Two modes of North American drought from instrumental and paleoclimatic data *J. Clim.* **22** 4336–47
- Yu S Coauthors 2014 Attribution of the United States “warming hole”: aerosol indirect effect and precipitable water vapor *Sci. Rep.* **4** 6929
- Zhang Q Coauthors 2020 Reforestation and surface cooling in temperate zones: mechanisms and implications *Glob. Change Biol.* **26** 3384–401
- Zhou S Coauthors 2021 Soil moisture–atmosphere feedbacks mitigate declining water availability in drylands *Nat. Clim. Change* **11** 38–44